The Journal of Chemical Physics ARTICLE scitation.org/journal/jcp

Transient absorption spectroscopy based on uncompressed hollow core fiber white light proves pre-association between a radical ion photocatalyst and substrate

Cite as: J. Chem. Phys. 158, 144201 (2023); doi: 10.1063/5.0142225
Submitted: 12 January 2023 • Accepted: 23 March 2023 •
Published Online: 10 April 2023

Ajeet Kumar,[1] Pavel Malevich,[1] Lars Mewes,[1] Shangze Wu,[2] Joshua P. Barham,[2] and Jürgen Hauer[1,a)]

AFFILIATIONS

[1] Department of Chemistry and Catalysis Research Center (CRC), School of Natural Sciences, Technical University of Munich, 85748 Garching, Germany

[2] Universität Regensburg, Fakultät für Chemie und Pharmazie, 93040 Regensburg, Germany

[a)] **Author to whom correspondence should be addressed:** juergen.hauer@tum.de.
URL: https://www.ch.nat.tum.de/dynspec/startseite/

ABSTRACT

We present a hollow-core fiber (HCF) based transient absorption experiment, with capabilities beyond common titanium:sapphire based setups. By spectral filtering of the HCF spectrum, we provide pump pulses centered at 425 nm with several hundred nJ of pulse energy at the sample position. By employing the red edge of the HCF output for seeding CaF_2, we obtain smooth probing spectra in the range between 320 and 900 nm. We demonstrate the capabilities of our experiment by following the ultrafast relaxation dynamics of a radical cationic photocatalyst to prove its pre-association with an arene substrate, a phenomenon that was not detectable previously by steady-state spectroscopic techniques. The detected preassembly rationalizes the successful participation of radical ionic photocatalysts in single electron transfer reactions, a notion that has been subject to controversy in recent years.

I. INTRODUCTION

Femtosecond Transient absorption (TA) spectroscopy is a technique to measure the dynamics of photophysical and photochemical events in real-time.[1–8] Femtosecond pump pulses should be compressed with tunable central wavelength to address the spectroscopic transitions of interest in the sample. Non-colinear optical parametric amplifiers (NOPAs) are well-established tools for this purpose. When pumped by titanium:sapphire (Ti:Sa) lasers,[4,9] NOPAs routinely deliver pulses with a tunable central wavelength between 450 and 770 nm.[9–11] The use of a pair of cylindrical lenses was shown to enhance the pulse bandwidth in the blue-green spectral region.[12] Pulses with lower central wavelengths require an additional frequency doubling step, which further complicates experimental designs and may be detrimental to pulse stability.[13–17] We address this problem by using the blue edge of a hollow-core fiber (HCF) white light continuum, seeded by an 800 nm, 25 fs pulse. While such a HCF continuum is a perfectly suited pump source, its spectrum near the fundamental is too structured to be used for probing purposes. In general, probe pulse pulses should ideally provide a broadband and flat detection window. This is typically achieved by white light generation inside crystalline materials, such as sapphire or CaF_2.[18] When using the Ti:Sa fundamental for seeding white light generation, the spectral region around 800 nm has to be truncated due to its large intensity (>100 times) compared to the white light spectrum. To solve this issue, researchers have employed notch filters[19] or custom-made dielectric mirrors[1] to attenuate the spectral region around the seeding wavelength. This approach reaches its limits for ultrabroadband probing windows, as the filters needed to attenuate the 800 nm seeding wavelength may also show undesired absorption bands in the UV–VIS. Alternatively, near-infrared (NIR) OPAs have been employed for seeding.[18,20–22] While this

approach readily provides seed light of wavelengths outside the desired probing range, it comes at the price of higher experimental complexity. We avoid such further complication in our setup by using the red-most edge of the HCF continuum (>900 nm) for super-continuum generation in a bulk material. This approach leads to smooth probing spectra in the range between 320 and 900 nm.

Both technological advancements of our setup—ultrashort blue excitation and broadband, smooth probe spectra—are advantageous when studying ultrafast relaxation in a solvated photocatalyst. Its role is to absorb light, ideally solar radiation, to then activate molecular substrates by excitation- or electron transfer. Photocatalysis finds diverse applications, such as water treatment, synthetic organic chemistry, and the life science industry.[23,24] Here, we study photocatalytically active visible-light absorbing tris(*p*-substituted)aryl aminium radical cations, first discovered by Walter *et al.*,[25] who isolated them as bench-stable salts. Owing to their facile synthetic availability, customizability, and the remarkable stability of their radical cation forms, triarylamines have enjoyed a rich history of applications both as functional materials and as oxidants in organic synthesis.[26–30] From a spectroscopic perspective, Tri(*p*-substituted)arylamines, such as tri([1,1′-biphenyl]-4-yl)amine (T*p*BPA),[31] show absorption in the visible spectral range in their radical cationic form T*p*BPA$^{\bullet+}$. This is due to a broad and featureless transition into a charge transfer state, posing a challenge for conventional femtosecond spectroscopy, as it shows oscillator strength throughout most of the visible spectral range and extends beyond 800 nm.[31] While photocatalytically-active radical ions receive increasing attention in their synthetic applications, the underlying mechanisms are a topic of ongoing debate.[32–36] The typically short-lived excited states of radical ions, such as T*p*BPA$^{\bullet+}$, rule out diffusional engagement with target substrates, meaning that a pre-complexation between the substrate and photocatalyst is a necessary but not yet unequivocally proven prerequisite. Although we were successful in detecting steady-state spectroscopic (UV–vis, EPR) changes upon mixing structurally related TCBPA$^{\bullet+}$ with chlorobenzene as the substrate (μ = 1.6 D) in our previous study, this was not the case for T*p*BPA$^{\bullet+}$ with mesitylene as a substrate of negligible dipole moment.[37] This might suggest that only assemblies of substrates with sufficient dipole moments can lead to noticeable perturbations in the steady-state spectra of radical ion photocatalysts.[38] Moreover, other studies involving ultrashort-lived radical cationic photocatalysts have not observed perturbations in their steady-state UV–vis spectra when adding excesses of substrate representative of the synthetic photochemical reaction conditions.[39,40] Employing the full capacity of our setup, we observe the entire energy transfer cascade within T*p*BPA$^{\bullet+}$ and explain the lack of productivity upon excitation of the lower-energy NIR bands. We confirm the existence of a preassembly by observing the quenching of T*p*BPA$^{\bullet+}$ by mesitylene on a sub-picosecond timescale. This demonstrates how ruling out radical ion photocatalyst–substrate preassemblies by a lack of change in their steady-state spectra is naive and how only transient absorption spectroscopy is conclusive.

II. EXPERIMENTAL DESIGN

The schematics of the TA setup are shown in Fig. 1. A commercial Ti:Sa laser amplifier (Coherent Legend Elite Duo), delivering 25 fs laser pulses at 800 nm central wavelength with 2.4 mJ per pulse at 5 kHz repetition rate, is used as a fundamental light source. Pointing deviations are minimized in a beam stabilization unit (Aligna, TEM Messtechnik). Pulse energies are attenuated down to 178 μJ by a combination of $\lambda/2$ plate (500–900 nm achr. B. Halle) and a thin film polarizer (at 70°, EKSMA Optics). White light generation is achieved by focusing the beam into a 1 m Hollow-Core Fiber (Ultrafast Innovations) with an inner-diameter of 250 μm.[41,42] The fiber is kept under static pressure of 1 atm of Argon (Ar) gas. The 800 nm pulses are focused into the fiber using a 1 m focal length plano-convex lens. The beam diameter at the lens's position is 10 mm. At the HCF entrance, the beam exhibits a $1/e^2$ beam waist of 120 μm, which amounts to less than 65% of the fiber's inner diameter.[43] The HCF output beam is collimated using a spherical mirror with 1 m focal length. Transmission efficiency is measured to be above 67% at the exit of the HCF with an output pulse energy of 120 μJ for the whole integrated spectrum. A dichroic beamsplitter (UV-cold mirror 45°, Thorlabs) is used to separate the Vis and NIR part of the HCF spectrum at 500 nm. The reflected visible part of the spectrum is then passed through a bandpass filter (CWL 438 nm, FWHM 40 nm, Edmund optics) and employed as a pump pulse. The filter is rotated with respect to the incoming beam to shift the central wavelength of the transmitted spectrum to 425 nm. This transmitted blue

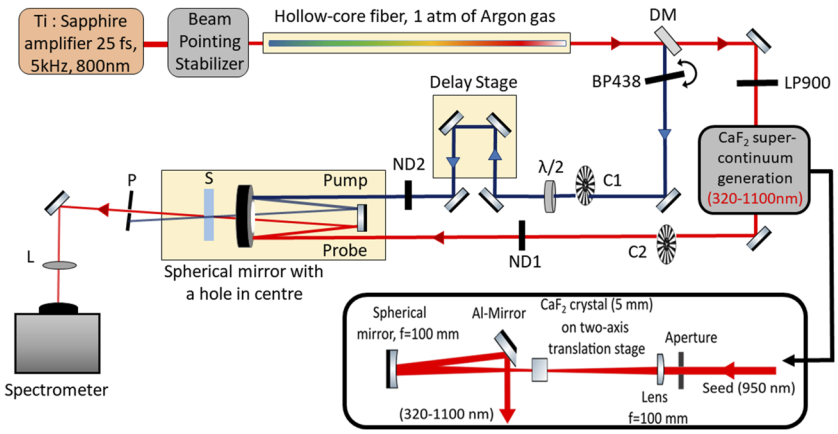

FIG. 1. Design of the HCF-based TA experiment: DM—dichroic mirror to reflect spectral components between 400 and 500 nm and transmit all wavelengths above 500 nm; BP425—bandpass filter (40 nm FWHM) to select the spectrum for pump (415–450 nm); LP900—longpass filter to select the spectrum for seed (900–1030 nm); C1 and C2—mechanical choppers; ND1 and ND2—neutral density filters; S—sample; L—focusing lens; and P—pinhole.

light passes via an all-reflective telescope consisting of a pair of two concave mirrors with focal lengths of 300 and 150 mm. The reflecting telescope reduces the beam waist by a factor of two, which, in turn, helps to keeps the pump beam diameter approximately four times bigger than the probe at the sample position. The telescope is omitted for clarity in Fig. 1. The transmitted long wavelength part of the spectrum between 600 and 1050 nm passes through a long-pass filter (900 nm, Premium long-pass filter, Thorlabs) and is used as seed to generate a super-continuum inside a continuously translated CaF_2 crystal. Details are given in Sec. III. After white light generation, aluminum mirrors are used to steer the beam to the sample position. Using a broadband half-wave plate ($\lambda/2$, 300–470 nm achr. B. Halle), the polarization of the pump pulse is set at magic angle (54.7°) with respect to the probe pulse.

Instead of typical single chopping, a double chopping scheme is used where both pump and probe pulses are modulated at a sub-harmonic frequency of the fundamental using two mechanical choppers (MC2000B, Thorlabs, C1 and C2 in Fig. 1), synchronized to the laser's repetition rate. Such a double chopping scheme is especially useful for the removal of pump-scattered light in inhomogenous samples.[44] Even for homogeneous samples as studied here, double chopping eases the interpretation and analysis of TA data near the pump wavelength as discussed in Sec. VI.[1,8] Both pump and probe pulses hit a spherical mirror (250 mm focal length) at an angle-of-incidence of ~0°. The pulses reflected from the spherical mirror hit a folding mirror, steering them through a hole in center of the spherical mirror. This optical design minimizes aberrations, such as astigmatism.[45] The $1/e^2$ beam waist of the focused pump and probe beam at the sample position is ~200 and 65 μm, respectively, as determined by a beam profiler (CMOS-1201, Cinogy). To attenuate the intensity of pump and probe pulses, 1 mm thick variable metallic neutral density filters (NDUV filter, Thorlabs) were used. For the measurements presented, we employed 6 nJ excitation energy per pump pulse. The probe pulse was more than 60 times weaker than the pump pulse. The pump pulse is delayed with respect to the probe pulse by a motorized linear stage (IMS300CCHA, Newport) with a minimum step size of 8 fs and 100% reproducibility and a maximal optical path length difference corresponding to two nanoseconds. After the sample, the transmitted probe pulse is focused onto an optical fiber (AVA FC-IR0100-2-ME, Avantes) with a core diameter of 100 μm using a 75 mm lens. The fiber is coupled to the entrance of a grating-based spectrometer (Kymera 328i, ANDOR), which is equipped with a CMOS camera (Zyla 4.2 plus, ANDOR). The spectrometer is equipped with two gratings, blazed at 500 and 800 nm, respectively. These gratings allow for spectral coverage between 350 and 1050 nm in two different measurements. The camera allows us to record the transmitted probe spectrum in shot-to-shot detection mode at the laser's repetition rate of 5 kHz.[17,46]

III. HOLLOW-CORE FIBER FOR BLUE EXCITATION AND SUPER-CONTINUUM PROBE LIGHT GENERATION

To optimize the blue components of the HCF spectrum, the choice of inert gas in the HCF is crucial.[41,47] Neon (Ne) has a higher ionization potential than Argon (Ar), which allows for higher input powers before the onset of ionization. While this results in a higher HCF output intensity, Ar yields broader output spectra as compared to Ne. Using Ne under our experimental conditions, the spectrum hardly reaches down to 450 nm, while the Ar spectrum extends down to 400 nm.[48] Hence, the HCF input intensity in Ar can be kept four times lower than for Ne while achieving broader spectra. We note that Liu *et al.*[49] also employed an Ar-filled HCF but seed it with the second harmonic of a Ti:Sa laser to achieve 8 fs pulses at 400 nm central wavelengths at the price of a more intricate experimental design. After optimizing system parameters, such as gas pressure and input power, we obtain 700 nJ pulses at the sample position at 425 nm central wavelength. The latter is obtained by a combination of dichroic mirror and bandpass filter as explained above.

We employ a 5 mm thick CaF_2 crystal for super-continuum generation.[18] The HCF-generated seed light with 950 nm central wavelength (see the dark gray spectrum in Fig. 2) is focused into the crystal using a 100 mm plano-convex lens. After the crystal, the light is collimated using a 100 mm aluminum coated spherical mirror; the choice of reflective optics avoids chromatic aberrations that would result from lenses and broadens the UV probing range. The astigmatism is minimized by keeping the angle between the incoming and the outgoing beam at a minimum of <5° by use of a D-shaped mirror. Damage to the CaF_2 crystal is avoided by moving it in an elliptical trace using a homemade two-axis motorized translation stage. It consists of two NEMA-17 stepper motors controlled by a code programmed on Arduino-uno. The spectrum of the super-continuum white light at the sample position is shown in Fig. 2 and measured using a fiber-coupled handheld spectrometer (Ocean Optics). The light gray line in Fig. 2 shows a typical HCF spectrum with its highly modulated 800 nm region. This part of the

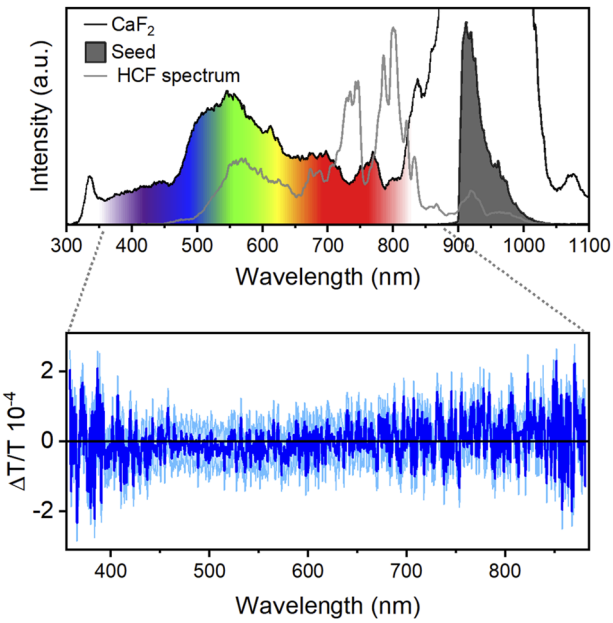

FIG. 2. Black line: CaF_2 super-continuum generated with the dark gray seed spectrum. Light gray line: spectrum of the HCF output. The $\Delta T/T$ spectrum is obtained with the pump beam blocked and represents the average over 4000 consecutive shots (blue line). The light blue area indicates the relative noise in terms of one standard deviation with a root mean square value of 1.3×10^{-4}.

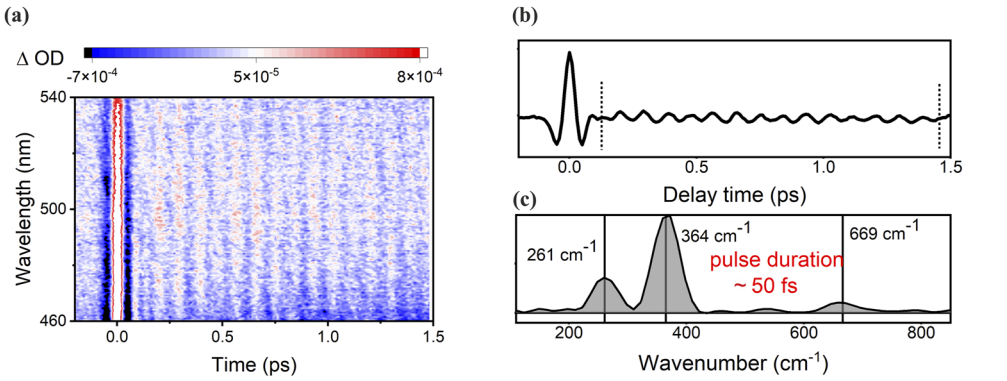

FIG. 3. Extracting normal modes of chloroform from impulsive vibrational spectroscopy. (a) Differential absorption map after dispersion correction in the range from 460 to 540 nm for clear visualization of vibrational wavepacket modulations. (b) Integration over all detection wavelengths followed by fast Fourier transformation of the selected part of the transient (dotted lines) leads to a Raman spectrum (c), the highest resolved frequency of which gives an upper estimate of the duration of the pump pulse.

spectrum is flattened by employing the red edge of the HCF continuum to seed white light in CaF_2. The resulting spectrum is shown as a partially filled black line in Fig. 2. Such a smooth probing spectrum is an important prerequisite for studying the charge transfer band dynamics of T*p*BPA$^{\bullet+}$ as discussed in Sec. VI. We note that the energy of the seed light after the longpass filter is sufficient to generate continuum not only in CaF_2 but also in YAG crystals (spectra not shown). The seed energy in the red part of the HCF spectrum can be increased further by filling the HCF chamber with Ne instead of Ar gas. This opens the possibility of extending the capabilities of our experiment to include probing in the NIR region.

IV. ESTIMATION OF PUMP-PULSE DURATION AND SIGNAL TO NOISE RATIO

In a previous realization of HCF-based TA,[31] we employed sub-10 fs pump pulses obtained by a chirped mirror compression stage. The reflectivity of the chirped mirrors did not allow for excitation spectra below 500 nm. In this work, the chirped mirrors are avoided to obtain excitation spectra in the 400–500 nm range. The omission of a dedicated pulse compression leaves the duration of the pump pulses in question. Autocorrelation,[50] second harmonic frequency resolved optical gating (SHG-FROG),[51] and transient grating FROG (TG-FROG)[52] are standard pulse characterization methods. Both autocorrelation and SHG-FROG require a nonlinear medium for frequency doubling, such as beta barium borate (BBO). The fact that the spectrum of the second harmonic of pulses with a center wavelength of 420 nm lies well within the absorption range of BBO rules out SHG-based approaches. TG-FROG measurements are also not applicable as they require higher pulse energies than available in our experiment. This leads us to impulsive stimulated Raman spectroscopy on pure solvents, such as choloroform,[1,4,53–56] to estimate the pulse duration of the pump *in situ*. The transient map for the measured data is shown in Fig. 3(a). Figure 3(b) shows the time trace of the dataset in Fig. 3(a) after integration over all detection wavelengths. Fast-Fourier transform (FFT) of this time trace leads to the vibrational frequency spectrum of Raman active ground state modes in chloroform accessible by the employed pump pulse. We note that the spectral phase of the pulse has to be flat in order to excite vibrational wavepackets efficiently.[53] Therefore, the mode of the highest frequency (669 cm^{-1}) obtained after FFT is an indicator of the duration of the pump pulse. From Fig. 3(c), we see that the 669 cm^{-1} mode is clearly resolved. This is only possible if the duration of the pump pulse is in the range of 50 fs (at a Fourier-limit of under 7 fs). 50 fs hence poses as an estimate for the pump pulse duration. To test the sensitivity of the setup, we block the pump beam and average the probe spectrum over 4000 consecutive shots.[4] Figure 2(b) shows the resulting ΔT/T spectrum. This presents the typical baseline for our setup corresponding to a (spectrally averaged) root mean square fluctuation of $\Delta T/T = 1.3 \times 10^{-4}$, which compares well with other experiments.[4,7] Inspection of Fig. 2(b) shows that the baseline converges correctly to zero.[7] The magnitude of the retrieved noise is depicted as one standard deviation of the 4000 shot average, depicted as the light-blue area in the lower panel of Fig. 2. The noise is not uniform over all detection wavelengths; this rules out referencing with photodiodes as they integrate the entire detection range.[7] Comparing the structure of the measured noise distribution for the HCF- and the CaF_2-retrieved white light reveals an advantage of using the 950 nm seed pulse. As shown in Fig. 4, the HCF output spectrum is strongly modulated around the 800 nm driving wavelength,

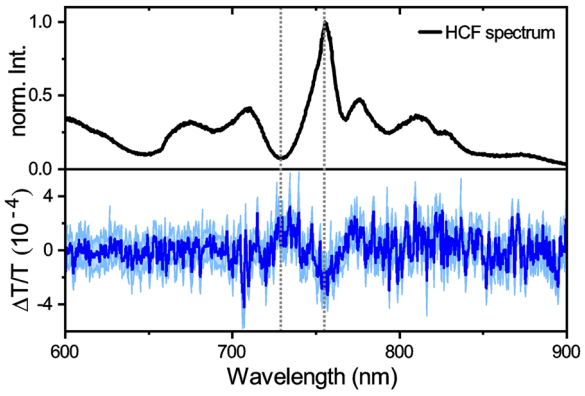

FIG. 4. Black line: HCF continuum spectrum recorded on the Andor CCD spectrometer. The ΔT/T spectrum is obtained with the pump beam blocked and represents the average over 4000 consecutive shots (blue line). The light blue area indicates the relative noise in terms of one standard deviation with a root mean square value of 1.9×10^{-4}. Noticeable systematic errors, i.e., deviations from zero, coincide with extrema in the HCF-spectrum, highlighted by gray vertical lines.

with pronounced extrema at the wavelengths indicated by the gray dashed lines. At these wavelengths of maximal/minimal HCF output intensity, the noise statistics (lower panel in Fig. 4) show systematic deviations from zero, which we attribute to low signal levels (HCF intensity minimum) or correlated shot-to-shot fluctuations (maximum).[57] The noise distribution for 950 nm seeded CaF_2-white light is uniform in comparison (see the lower panel in Fig. 2).

V. SAMPLE PREPARATION, MEASUREMENTS, AND DATA PROCESSING

To demonstrate the capabilities of our setup, we choose T*p*BPA$^{\bullet+}$ in the form of its hexafluorophosphate salt as a test sample in the absence and presence of a photocatalytic substrate, i.e., mesitylene. The aims are to decipher energy transfer pathways of the catalyst (T*p*BPA$^{\bullet+}$) and to find evidence for pre-association between the substrate and the catalyst. The latter will manifest as changes of the ultrafast dynamics after addition of the substrate. The absorption spectrum of solvated T*p*BPA$^{\bullet+}$ is shown as a black line in Fig. 5 and exhibits a transition associated with the π–electron system in the blue spectral range, covered by the employed pump pulse (blue line in Fig. 5). Importantly, this transition is completely absent in the neutral form T*p*BPA, ensuring that all subsequent TA data stem from T*p*BPA$^{\bullet+}$ and not to T*p*BPA. An additional broad absorptive feature between 600 and 1000 nm is associated with a charge transfer band. The width of this band and the fact that it extends beyond 800 nm render this sample difficult for conventional TA experiments. The synthetic route and purification-related information of T*p*BPA and T*p*BPA$^{\bullet+}$ are found in Ref. 31. For the TA-measurements, the sample was dissolved in dichloromethane (DCM) purchased from Sigma-Aldrich. The solvent was dried by molecular sieves to prevent a gradual sample degradation in solution in the ground state when exposed to atmosphere/water. For the sample of T*p*BPA$^{\bullet+}$ in the presence of its target substrate, 350 equivalents of mesitylene were added to the T*p*BPA$^{\bullet+}$ solution. This excess mirrors the synthetic photoelectrochemical reaction conditions, in which T*p*BPA is employed in a catalytic loading. The sample was kept in the dark for 40 min. prior to TA measurements. This is to allow adequate time for a non-covalent pre-complex to form between T*p*BPA$^{\bullet+}$ and mesitylene, hypothesized in our previous study[31] and confirmed herein (*vide infra*). All the measurements were finished within three hours after sample preparation and performed using a 1 mm thick cuvette with a Polytetrafluoroethylene (PTFE) airtight. During the TA measurements, the cuvette was continuously moved perpendicularly to the laser beam path in order to avoid photodamage or photo-bleaching of the sample. No degradation of the absorption spectrum was observed when comparing spectra before and after the TA measurements. Absorption difference spectra were recorded at different pump–probe delays from −1 to 100 ps. The initial −1 to 1 ps were recorded with 10 fs step size. For longer time delays, the step size was logarithmic in order to reduce data acquisition time without compromising data quality. In all TA spectra, the chirp of the white-light super-continuum was corrected. In order to analyze the underlying molecular kinetics, global analysis (GA) was performed using Glotaran.[58] Data for time delays shorter than 70 fs were disregarded to exclude the coherent artifact in the pump–probe pulse overlap region.[59] A three component sequential model was used to fit the TA data between 70 fs and 100 ps.

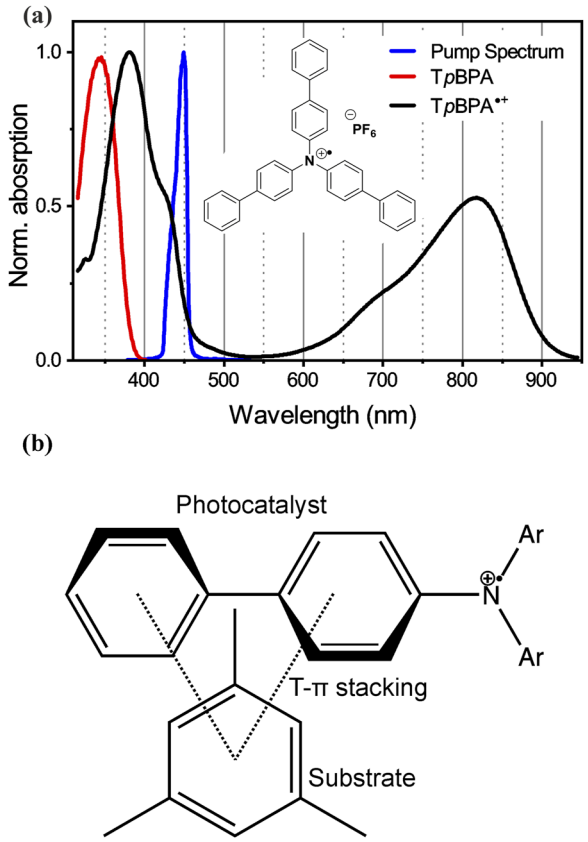

FIG. 5. (a) Absorption spectrum of T*p*BPA$^{\bullet+}$ (black line), pump pulse spectrum (blue), and neutral form of T*p*BPA$^{\bullet+}$ (red) with the indicated molecular structure. (b) T*p*BPA$^{\bullet+}$ is proposed to form a non-covalent precomplex with mesitylene via a T–π stacking interaction.[31]

VI. RESULTS AND DISCUSSION

From our previous study,[31] we know that the photocatalyst in its neutral form, i.e., T*p*BPA, shows a strong absorption band at 345 nm [see Fig. 5(a), red line]. In the radical cationic form, T*p*BPA$^{\bullet+}$, this band disappears and two new bands between 360–430 and 600–900 nm appear, shown as the black spectrum in Fig. 5(a). When using T*p*BPA$^{\bullet+}$ as a photocatalyst, no downstream C(sp^2)-N coupled product was observed upon excitation at 721 nm (0% yield) and 856 nm (0%), while 365 nm excitation, at which the neutral precursor T*p*BPA also absorbs, led to only a very low yield (11%). Excitation at 394 nm, however, leads to a product yield of 88%. Clearly, only certain higher-lying states in the radical cation are relevant in the photocatalytic mechanism. It is also known from the literature that the excited state lifetime of the charge transfer band is on the order of several picoseconds,[31] which is incompatible with a diffusion controlled mechanism. The working hypothesis is hence pre-association between the photocatalyst (T*p*BPA$^{\bullet+}$) and the substrate (mesitylene), as depicted in Fig. 5(b). The lifetime of the higher-lying excited states in T*p*BPA$^{\bullet+}$ is still unknown. Hence,

we investigate the lifetime of the state after 420 nm excitation, where absorption of the neutral form is negligible and the photocatalytic yield is high. In an effort to quantify the quenching efficiency—and therewith to prove or disprove possible pre-association between the substrate and the catalyst—we excite the 420 nm band of T*p*BPA$^{\bullet+}$ in the absence and presence of mesitylene. The contour map for the TA signal for T*p*BPA$^{\bullet+}$ is shown in Fig. 6(a). The negative signal centered around 420 and 880 nm stems from ground state bleach (GSB) and stimulated emission (SE), while the positive signal in the range of 450–700 nm is attributed to excited-state absorption (ESA). Within 40 ps, all excited states deactivate completely back to the electronic ground state. The kinetics taken at 420 nm [see dashed indicators in Fig. 6(a)] are shown in Fig. 6(b). We note that addition of mesitylene to T*p*BPA$^{\bullet+}$ does not change the steady-state absorption spectrum.[31] Accordingly, the overall TA-signal remains largely unchanged. The early decay dynamics, however, are significantly affected by addition of the substrate, as shown in Fig. 6(b). Kinetics at 420 nm with the substrate [red curves in Fig. 6(b)] show significant quenching. This behavior is a strong indication that quenching effects are most pronounced for the higher lying states (420 nm) but are negligible for the lower lying charge transfer state. We also observe wavepacket modulation as oscillatory deviations from the kinetic fit, shown as faint gray and red lines in Fig. 6(b). Details of the kinetic fit by GA are given below. Fourier-transformation of the oscillatory signal part after zero-padding and background subtraction show an intricate frequency spectrum, as depicted in the lower panel of Fig. 6(b), but no significant difference in the absence or presence of the substrate. We conclude that pre-association changes the ultrafast kinetics but does not alter the normal modes of T*p*BPA$^{\bullet+}$ appreciably. Spectral cuts at indicated delay times draw a similar picture: the initial decay is slower without the substrate [see Fig. 6(c) vs Fig. 6(d)], while the overall spectral shape is conserved.

We quantify the observed quenching effects by applying GA using a sequential model to the data with and without mesitylene. Results were obtained using the GLOTARAN package[58] and are shown in Fig. 7. Figures 7(a) and 7(b) show the Evolution Associated Spectra (EAS) for T*p*BPA$^{\bullet+}$ and T*p*BPA$^{\bullet+}$ + mesitylene, respectively. In both cases, three species were sufficient to achieve a satisfactory fit. We note that the amplitude of the third species (EAS3) is very low compared to EAS1 and EAS2 in both cases. Further inspection of the lifetime of the obtained species leads to the following conclusive picture: without substrate, we obtain three different lifetimes with τ_1 (0.92 ps), τ_2 (4.8 ps), and τ_3 (26.7 ps). In the presence of the substrate, we find the same number of decay components: τ_1 (0.34 ps), τ_2 (4.8 ps), and τ_3 (18 ps) but with a markedly shorter lifetime for components one and three. The decay component of 4.8 ps in both the cases remains unchanged and also matches with the reported value when pumping and probing in the charge transfer band region.[31] τ_1 is decreased by a factor of nearly three in the presence of the substrate, as also shown in Figs. 7(c) and 7(d). This finding explains why the higher-lying state at 420 nm is the only state that significantly contributes to the photocatalytic reaction. Furthermore, this proves that pre-association between T*p*BPA$^{\bullet+}$ and mesitylene occurs, even though such a pre-association could not be detected by UV–vis and EPR spectroscopy.[31] This demonstrates a key advantage of the TA experiment presented here in probing the mechanisms of radical ion photocatalytic reactions. In contrast, the lack of quenching effects on τ_2—associated with the charge transfer state—highlights that excitation of this state leads to no product for-

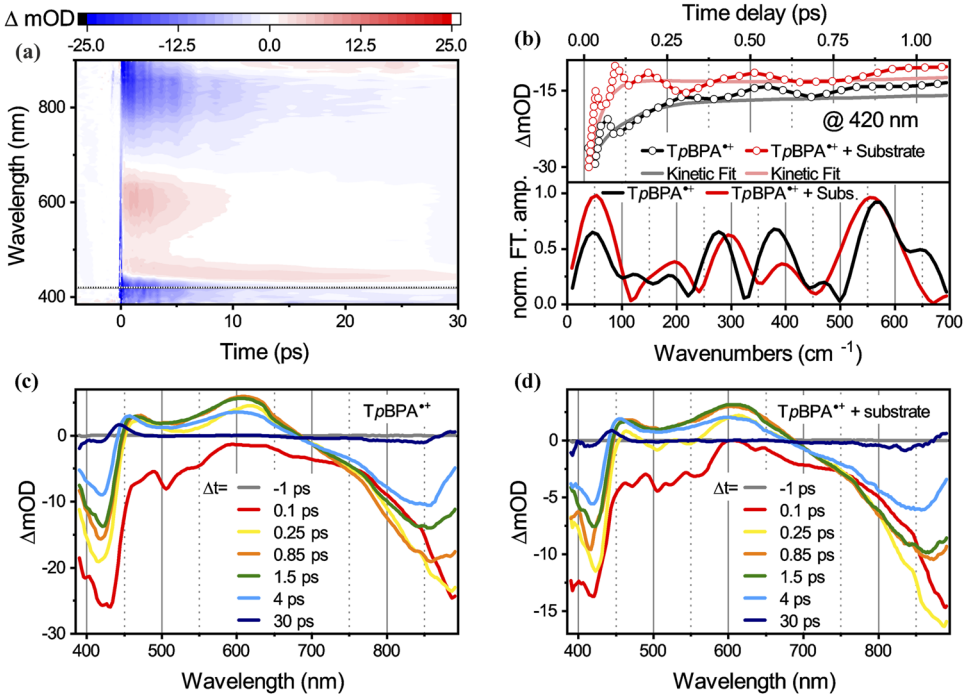

FIG. 6. (a) Contour plot for TA data of T*p*BPA$^{\bullet+}$ dissolved in dichloromethane (DCM). The positive (negative) signals stem from excited state absorption (ground state bleach and stimulated emission) and are shown in red (blue) colors. (b) Decay kinetics at 420 nm detection wavelength for T*p*BPA$^{\bullet+}$ in DCM with (red circles) and without (black circles) substrate (350 equivalents of the mesitylene). Solid faint black and red lines present the kinetics fit from global analysis. (c) and (d) show spectral cuts at the indicated delay times without and with substrate. We note that the change in the TA-signal between (c) and (d) is due to lower catalyst concentration after substrate addition.

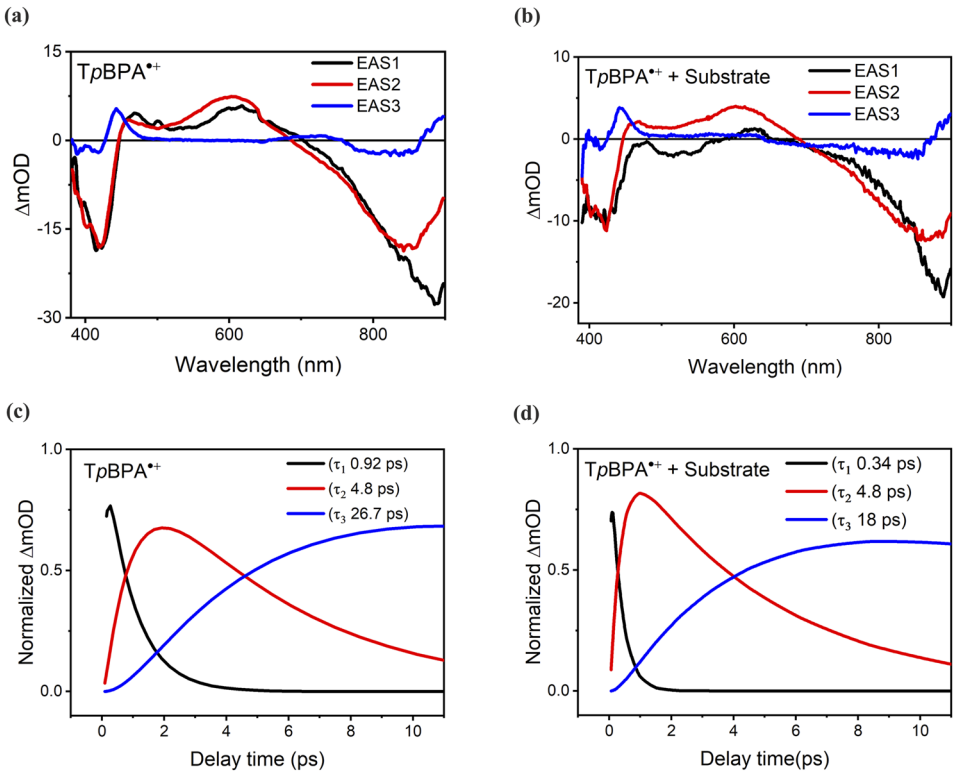

FIG. 7. (a) T*p*BPA$^{\bullet+}$ evolution associated spectra (EAS) without substrate, (b) T*p*BPA$^{\bullet+}$ EAS with substrate, (c) T*p*BPA$^{\bullet+}$ temporal species concentration profiles, and (d) T*p*BPA$^{\bullet+}$ temporal species concentration profiles with substrate.

mation in photocatalytic experiments. As the lifetime of this state in the single picosecond range is too short to support diffusion limited processes, pre-association with the substrate would be the only possible route for photocatalytic activity. τ_3 is a low-amplitude feature, which may be ascribed to photoproduct formation or other long-lived states, which we exclude from further analysis. Pre-association with mesitylene provides an additional decay channel for electron transfer from T*p*BPA$^{\bullet+}$ to the substrate. The fact that we do not detect an additional ESA feature, associated with an excited state in mesitylene after electron transfer (a radical cation), is not surprising as the presumably weak features of the mesitylene radical cation (with GSB in the deep UV) will be covered by the stronger ESA transitions of T*p*BPA$^{\bullet+}$.[60–62] By the change of excited state lifetime upon addition of the substrate, we can quantify the quenching efficiency, assuming that the decay rate of the higher-lying state in the presence and absence of the substrate is k_{complex} and k_{catalyst}, respectively. The rate of transfer from T*p*BPA$^{\bullet+}$ to the mesitylene $k_{\text{substrate}}$ can be defined by the following relation:

$$k_{\text{complex}} = k_{\text{catalyst}} + k_{\text{substrate}} \tag{1}$$

or

$$\frac{1}{\tau_{\text{complex}}} = \frac{1}{\tau_{\text{catalyst}}} + \frac{1}{\tau_{\text{substrate}}}. \tag{2}$$

The value of k_{complex} and k_{catalyst} is 1/0.34 and 1/0.92 ps, respectively. Now, using Eq. (2), we calculate $k_{\text{substrate}} = 1/\tau_{\text{substrate}} = 1/538\ \text{ps}^{-1}$, which amounts to 59% of k_{complex}.

VII. CONCLUSION

In this work, we have successfully employed HCF supercontinuum pulses in a versatile TA experiment. We achieved excitation with sub 50 fs, 425 nm pulses without a pulse compression unit. In terms of probing, we present a smooth spectrum between 320 and 900 nm by seeding with the red edge of the HCF supercontinuum. We apply this apparatus to a radical ion photocatalyst system and prove for the first time—based on kinetic arguments—pre-association between a radical cationic photocatalyst and substrate. This demonstrates the crucial importance of transient absorption spectroscopy for confirming/refuting radical ion photocatalyst–substrate assemblies when these cannot be detected by steady-state spectroscopic methods (UV–vis and EPR). Our study shows that it would be naïve to rule out such assemblies by a lack of perturbations in the steady-state spectra of radical ion catalysts in the presence of their target substrates. While the notion of radical ionic photocatalysts participating in single electron transfer reactions is a topic of notable controversy in recent years, our data support this notion being enabled by preassemblies.

ACKNOWLEDGMENTS

The project was funded by the Deutsche Forschungsgemeinschaft (DFG, German Research Foundation) (Grant No. TRR 325 – 444632635) and by Project No. 514636421. A.K. and J.H. acknowledges funding by the DFG under Germany's Excellence Strategy (Grant No. EXC 2089/1-390776260). S.W. and J.B. acknowledge funding by the Alexander von Humboldt Foundation within the

framework of the Sofja Kovalevskaja Award endowed to J.B. by the German Federal Ministry of Education and Research.

AUTHOR DECLARATIONS

Conflict of Interest

The authors have no conflicts to disclose.

Author Contributions

Ajeet Kumar: Data curation (equal); Formal analysis (equal); Methodology (equal); Visualization (equal); Writing – original draft (equal). **Pavel Malevich**: Conceptualization (equal); Supervision (equal); Writing – review & editing (equal). **Lars Mewes**: Supervision (equal); Validation (equal); Writing – review & editing (equal). **Shangze Wu**: Data curation (equal); Investigation (equal). **Joshua P. Barham**: Data curation (equal); Writing – review & editing (equal). **Jürgen Hauer**: Conceptualization (equal); Funding acquisition (equal); Methodology (equal); Supervision (equal); Writing – review & editing (equal).

DATA AVAILABILITY

The data that support the findings of this study are available from the corresponding author upon reasonable request.

REFERENCES

[1] U. Megerle, I. Pugliesi, C. Schriever, C. F. Sailer, and E. Riedle, Appl. Phys. B **96**, 215 (2009).
[2] R. Berera, R. van Grondelle, and J. T. M. Kennis, Photosynth. Res. **101**, 105 (2009).
[3] A. L. Dobryakov, S. A. Kovalenko, A. Weigel, J. L. Pérez-Lustres, J. Lange, A. Müller, and N. P. Ernsting, Rev. Sci. Instrum. **81**, 113106 (2010).
[4] D. Polli, L. Lüer, and G. Cerullo, Rev. Sci. Instrum. **78**, 103108 (2007).
[5] M. Maiuri, M. Garavelli, and G. Cerullo, J. Am. Chem. Soc. **142**, 3 (2020).
[6] A. Grupp, A. Budweg, M. P. Fischer, J. Allerbeck, G. Soavi, A. Leitenstorfer, and D. Brida, J. Opt. **20**, 014005 (2018).
[7] J. Brazard, L. A. Bizimana, and D. B. Turner, Rev. Sci. Instrum. **86**, 053106 (2015).
[8] B. Lang, Rev. Sci. Instrum. **89**, 093112 (2018).
[9] E. Riedle, M. Beutter, S. Lochbrunner, J. Piel, S. Schenkl, S. Spörlein, and W. Zinth, Appl. Phys. B **71**, 457 (2000).
[10] T. Wilhelm, J. Piel, and E. Riedle, Opt. Lett. **22**, 1494 (1997).
[11] P. Baum, S. Lochbrunner, L. Gallmann, G. Steinmeyer, U. Keller, and E. Riedle, Appl. Phys. B **74**, s219 (2002).
[12] P. J. M. Johnson, V. I. Prokhorenko, and R. J. D. Miller, Opt. Lett. **36**, 2170 (2011).
[13] M. Liebel, C. Schnedermann, and P. Kukura, Opt. Lett. **39**, 4112 (2014).
[14] P. Baum, S. Lochbrunner, and E. Riedle, Appl. Phys. B **79**, 1027 (2004).
[15] I. Kozma, P. Baum, S. Lochbrunner, and E. Riedle, Opt. Express **11**, 3110 (2003).
[16] M. Beutler, M. Ghotbi, F. Noack, D. Brida, C. Manzoni, and G. Cerullo, Opt. Lett. **34**, 710 (2009).
[17] E. Keil, P. Malevich, and J. Hauer, Opt. Express **29**, 39042 (2021).
[18] M. Bradler, P. Baum, and E. Riedle, Appl. Phys. B **97**, 561 (2009).
[19] U. Schmidhammer, P. Jeunesse, G. Stresing, and M. Mostafavi, Appl. Spectrosc. **68**, 1137 (2014).
[20] R. B. Varillas, A. Candeo, D. Viola, M. Garavelli, S. De Silvestri, G. Cerullo, and C. Manzoni, Opt. Lett. **39**, 3849 (2014).
[21] V. R. Policht, A. Niedringhaus, and J. P. Ogilvie, J. Phys. Chem. Lett. **9**, 6631 (2018).
[22] E. Riedle, M. Bradler, M. Wenninger, C. F. Sailer, and I. Pugliesi, Faraday Discuss. **163**, 139 (2013).
[23] G. Masson and B. König, Eur. J. Org. Chem. **2020**, 1191.
[24] L. Candish, K. D. Collins, G. C. Cook, J. J. Douglas, A. Gómez-Suárez, A. Jolit, and S. Keess, Chem. Rev. **122**, 2907 (2022).
[25] R. I. Walter, J. Am. Chem. Soc. **77**, 5999 (1955).
[26] Z. Ning and H. Tian, Chem. Commun. **2009**, 5483.
[27] R. A. Pabon, D. J. Bellville, and N. L. Bauld, J. Am. Chem. Soc. **105**, 5158 (1983).
[28] U. Jahn and S. Aussieker, Org. Lett. **1**, 849 (1999).
[29] J. P. Barham, M. P. John, and J. A. Murphy, J. Am. Chem. Soc. **138**, 15482 (2016).
[30] R. Francke and R. D. Little, Chem. Soc. Rev. **43**, 2492 (2014).
[31] S. Wu, J. Žurauskas, M. Domański, P. S. Hitzfeld, V. Butera, D. J. Scott, J. Rehbein, A. Kumar, E. Thyrhaug, J. Hauer, and J. P. Barham, Org. Chem. Front. **8**, 1132 (2021).
[32] X. Tian, T. A. Karl, S. Reiter, S. Yakubov, R. de Vivie-Riedle, B. König, and J. P. Barham, Angew. Chem., Int. Ed. Engl. **60**, 20817 (2021).
[33] D. Y. Jeong, D. S. Lee, H. L. Lee, S. Nah, J. Y. Lee, E. J. Cho, and Y. You, ACS Catal. **12**, 6047 (2022).
[34] S. Wu, J. Kaur, T. A. Karl, X. Tian, and J. P. Barham, Angew. Chem., Int. Ed. **61**, e202107811 (2022).
[35] J. S. Beckwith, A. Aster, and E. Vauthey, Phys. Chem. Chem. Phys. **24**, 568 (2022).
[36] M. J. P. Mandigma, J. Kaur, and J. P. Barham, ChemCatChem (published online 2023).
[37] O. W. Kolling, Trans. Kans. Acad. Sci. **98**, 113 (1995).
[38] S. Wu *et al.*, Org. Chem. Front. **8**, 1132–1142 (2021).
[39] K. Targos, O. P. Williams, and Z. K. Wickens, J. Am. Chem. Soc. **143**, 4125 (2021).
[40] D. Rombach and H.-A. Wagenknecht, ChemCatChem **10**, 2955 (2018).
[41] M. Nisoli, S. De Silvestri, O. Svelto, R. Szipöcs, K. Ferencz, C. Spielmann, S. Sartania, and F. Krausz, Opt. Lett. **22**, 522 (1997).
[42] X. Ma, J. Dostál, and T. Brixner, Opt. Express **24**, 20781 (2016).
[43] E. A. J. Marcatili and R. A. Schmeltzer, Bell Syst. Tech. J. **43**, 1783 (1964).
[44] J. Dostál, J. Pšenčík, and D. Zigmantas, Nat. Chem. **8**, 705 (2016).
[45] A. Nemeth, J. Sperling, J. Hauer, H. F. Kauffmann, and F. Milota, Opt. Lett. **34**, 3301 (2009).
[46] F. Kanal, S. Keiber, R. Eck, and T. Brixner, Opt. Express **22**, 16965 (2014).
[47] W. A. Okell, T. Witting, D. Fabris, D. Austin, M. Bocoum, F. Frank, A. Ricci, A. Jullien, D. Walke, J. P. Marangos, R. Lopez-Martens, and J. W. G. Tisch, Opt. Lett. **38**, 3918 (2013).
[48] D. Wang, Y. Leng, and Z. Xu, Appl. Phys. B **111**, 447 (2013).
[49] J. Liu, Y. Kida, T. Teramoto, and T. Kobayashi, Opt. Express **18**, 4664 (2010).
[50] J. K. Ranka, A. L. Gaeta, A. Baltuska, M. S. Pshenichnikov, and D. A. Wiersma, Opt. Lett. **22**, 1344 (1997).
[51] K. W. DeLong, R. Trebino, J. Hunter, and W. E. White, J. Opt. Soc. Am. B **11**, 2206 (1994).
[52] R. Trebino, K. W. DeLong, D. N. Fittinghoff, J. N. Sweetser, M. A. Krumbügel, B. A. Richman, and D. J. Kane, Rev. Sci. Instrum. **68**, 3277 (1997).
[53] M. Liebel, C. Schnedermann, T. Wende, and P. Kukura, J. Phys. Chem. **119**, 9506 (2015).
[54] S. Dhamija, G. Bhutani, A. Jayachandran, and A. K. De, J. Phys. Chem. A **126**, 1019 (2022).
[55] G. Batignani, C. Ferrante, G. Fumero, and T. Scopigno, J. Phys. Chem. Lett. **10**, 7789 (2019); arXiv:1911.12086.
[56] D. W. McCamant, P. Kukura, S. Yoon, and R. A. Mathies, Rev. Sci. Instrum. **75**, 4971 (2004).
[57] M. Bradler and E. Riedle, J. Opt. Soc. Am. B **31**, 1465 (2014).
[58] I. H. M. van Stokkum, D. S. Larsen, and R. van Grondelle, Biochim. Biophys. Acta, Bioenerg. **1657**, 82 (2004).
[59] M. Lorenc, M. Ziolek, R. Naskrecki, J. Karolczak, J. Kubicki, and A. Maciejewski, Appl. Phys. B **74**, 19 (2002).
[60] K. Sehested, J. Holcman, and E. J. Hart, J. Phys. Chem. **81**, 1363 (1977).
[61] S. M. Hubig and J. K. Kochi, J. Am. Chem. Soc. **122**, 8279 (2000).
[62] P. B. Merkel, P. Luo, J. P. Dinnocenzo, and S. Farid, J. Org. Chem. **74**, 5163 (2009).